1-1-2005

Infrared refractive indices of liquid crystals

Jun Li
University of Central Florida

Shin-Tson Wu
University of Central Florida

Stefano Brugioni

Riccardo Meucci

Sandro Faetti

Infrared refractive indices of liquid crystals

Cite as: J. Appl. Phys. **97**, 073501 (2005); https://doi.org/10.1063/1.1877815
Submitted: 04 January 2005 . Accepted: 01 February 2005 . Published Online: 18 March 2005

Jun Li, Shin-Tson Wu, Stefano Brugioni, Riccardo Meucci, and Sandro Faetti

Infrared refractive indices of liquid crystals

Jun Li and Shin-Tson Wu[a)]
College of Optics and Photonics, University of Central Florida, Orlando, Florida 32816

Stefano Brugioni and Riccardo Meucci
Istituto Nazionale di Ottica Applicata, Largo E. Fermi 6-50125 Firenze, Italy

Sandro Faetti
Dipartimento di Fisica dell'Universita' di Pisa, Via Buonarroti 2, 56127 Pisa, Italy

(Received 4 January 2005; accepted 1 February 2005; published online 18 March 2005)

The refractive indices of E7 liquid-crystal mixture were measured at six visible and two infrared ($\lambda = 1.55$ and $10.6\ \mu$m) wavelengths at different temperatures, using Abbe and wedged cell refractometer methods, respectively. The experimental data of the visible wavelengths fit the extended Cauchy equations well. Using the extended Cauchy equations, we can extrapolate the refractive indices of E7 to IR. The extrapolated results almost strike through the measured data. Thus, the extended Cauchy equations can be used to link the visible refractive indices to infrared, where the refractive index measurements are more difficult. © *2005 American Institute of Physics*. [DOI: 10.1063/1.1877815]

I. INTRODUCTION

Liquid crystal (LC) possesses a relatively large birefringence ($\Delta n = n_e - n_o$) in the infrared (IR) region[1,2] and has been used extensively for dynamic scene projectors,[3] laser beam steering,[4,5] tunable band-gap photonic crystal fibers,[6,7] and millimeter-wave electronic phase shifters.[8,9] Simple methods, such as voltage- or wavelength-dependent phase retardation methods, have been developed for measuring the IR birefringence of LCs.[10] However, only few methods, e.g., the Talbot–Rayleigh refractometer[11] and wedged cell refractometer,[12,13] are available for measuring the individual extraordinary (n_e) and ordinary (n_o) refractive indices in the IR region. Moreover, these measurements are tedious because the IR refractometer is harder to align precisely and most of the moisture-resistant IR substrates are not transparent in the visible so that visual inspection of LC alignment quality and cell uniformity is more difficult.

By contrast, in the visible spectral region the LC refractive indices can be measured quite easily by the commercial Abbe refractometer. Its accuracy is up to the fourth decimal point (±0.0002). However, the usable range of Abbe refractometer is limited to visible and near IR because of the faint refractive light from the main prism and the transparency of the prism.

In this paper, we link the visible and IR refractive indices by the extended Cauchy equations. First, we measured the refractive indices of E7 LC mixture at six visible wavelengths using an Abbe refractometer and two IR wavelengths ($\lambda = 1.55$ and $10.6\ \mu$m) using a wedged cell refractometer. We fit the visible refractive index data with the extended Cauchy equation. Once the three Cauchy coefficients are obtained, we use the extended Cauchy equations to extrapolate the refractive indices to the IR wavelengths. These extrapolated data almost strike through the experimental results. In Sec. II, we briefly review the extended Cauchy model for describing the wavelength and temperature effects of the LC refractive indices. In Sec. III, we describe the Abbe and wedged cell refractometers for measuring the visible and IR refractive indices. In Sec. IV, we link these two sets of experimental data by the extended Cauchy equations. Excellent agreement between the model and experiment is found.

II. THEORY

The LC refractive indices are mainly determined by the molecular structures, wavelength, and temperature. Most of these effects have been reported previously. Here, we briefly summarize the wavelength and temperature effects in order to compare with the experimental results.

A. Wavelength effect

The major absorption of a LC compound occurs in two spectral regions: ultraviolet (UV) and IR.[12] The $\sigma \rightarrow \sigma^*$ electronic transition takes place in the vacuum UV (100–180 nm) region whereas the $\pi \rightarrow \pi^*$ electronic transition occurs, in the UV (180–400 nm) region. If a LC molecule has a longer conjugation, its electronic transition wavelength would extend to a longer UV wavelength. In the near IR region, some overtone molecular vibration bands appear.[14] The fundamental molecular vibration bands, such as CH, CN, and C=C, occur in the mid and long IR regions. Typically, the oscillator strength of these vibration bands is about two orders of magnitude weaker than that of the electronic transitions. Thus, the resonant enhancement of these bands to the LC birefringence is localized.[15]

The three-band model[16] was derived based on the LC absorption spectra. It takes the three main electronic transitions into consideration: one $\sigma \rightarrow \sigma^*$ transition (the λ_0-band) and two $\pi \rightarrow \pi^*$ transitions (the λ_1-band and λ_2-band). In the three-band model, the refractive indices (n_e and n_o) are expressed as follows:[16]

[a)]Electronic mail: swu@mail.ucf.edu

$$n_e \cong 1 + g_{0e}\frac{\lambda^2\lambda_0^2}{\lambda^2-\lambda_0^2} + g_{1e}\frac{\lambda^2\lambda_1^2}{\lambda^2-\lambda_1^2} + g_{2e}\frac{\lambda^2\lambda_2^2}{\lambda^2-\lambda_2^2}, \tag{1a}$$

$$n_o \cong 1 + g_{0o}\frac{\lambda^2\lambda_0^2}{\lambda^2-\lambda_0^2} + g_{1o}\frac{\lambda^2\lambda_1^2}{\lambda^2-\lambda_1^2} + g_{2o}\frac{\lambda^2\lambda_2^2}{\lambda^2-\lambda_2^2}. \tag{1b}$$

The three-band model describes the refractive index origins of LC compounds. However, a commercial mixture usually consists of several compounds with different structures. The individual λ_i's are quite different so that Eq. (1) would have too many unknowns to describe the refractive indices of a LC mixture.

To model the refractive indices for LC mixtures, we could expand Eq. (1) into power series because in the visible and IR wavelengths, $\lambda \gg \lambda_2$. By keeping up to the λ^{-4} terms, we derive the extended Cauchy model,[17]

$$n_e \cong A_e + \frac{B_e}{\lambda^2} + \frac{C_e}{\lambda^4}, \tag{2a}$$

$$n_o \cong A_o + \frac{B_o}{\lambda^2} + \frac{C_o}{\lambda^4}. \tag{2b}$$

Although Eq. (2) is derived based on a LC compound, it can be extended easily to eutectic mixtures by taking the superposition of each compound.[17] Equation (2) applies equally well to both high and low birefringence LC materials. For low birefringence LC mixtures, the λ^{-4} terms are insignificant and can be omitted, thus, n_e and n_o each has only two parameters.[18]

From Eq. (2), if we measure the refractive indices at three wavelengths, then the three Cauchy coefficients ($A_{e,o}$, $B_{e,o}$, and $C_{e,o}$) can be obtained by fitting the experimental results. Once these coefficients are determined, the refractive indices at any wavelength can be calculated. From Eq. (2), the refractive indices and birefringence decrease as the wavelength increases. In the long-wavelength region, n_e and n_o are reduced to A_e and A_o, respectively. The coefficients A_e and A_o are constants; they are independent of the wavelength, but dependent on the temperature. That means, in the IR region the refractive indices are insensitive to the wavelength, except near the local molecular vibration bands.

B. Temperature effect

The temperature effect of the LC refractive indices can be expressed by the average refractive index $\langle n\rangle$ and birefringence Δn as[19]

$$n_e = \langle n\rangle + \frac{2}{3}\Delta n, \tag{3a}$$

$$n_o = \langle n\rangle - \frac{1}{3}\Delta n. \tag{3b}$$

On the other hand, birefringence is dependent on the order parameter S. Based on Haller's approximation, the temperature-dependent birefringence has the following form:[20]

$$\Delta n(T) = (\Delta n)_o(1 - T/T_c)^{\beta}. \tag{4}$$

In Eq. (4), $(\Delta n)_o$ is the LC birefringence in the crystalline state (or $T=0$ K), the exponent β is a material constant, and T_c is the clearing temperature of the LC material under investigation. The average refractive index decreases linearly with increasing temperature as

$$\langle n\rangle = A - BT. \tag{5}$$

Substituting Eqs. (4) and (5) back to Eqs. (3a) and (3b), we derive the four-parameter model for describing the temperature dependence of the LC refractive indices,[21]

$$n_e(T) \approx A - BT + \frac{2(\Delta n)_o}{3}\left(1 - \frac{T}{T_c}\right)^{\beta}, \tag{6a}$$

$$n_o(T) \approx A - BT - \frac{(\Delta n)_o}{3}\left(1 - \frac{T}{T_c}\right)^{\beta}. \tag{6b}$$

Although Eq. (6) has four parameters, we can get $[A,B]$ and $[(\Delta n)_o,\beta]$, respectively, by two-stage fittings. To obtain $[A,B]$, we fit the average refractive index $\langle n\rangle = (n_e + 2n_o)/3$ as a function of temperature using Eq. (5). To find $[(\Delta n)_o,\beta]$, we fit the birefringence data as a function of temperature using Eq. (4). Therefore, these two sets of parameters can be obtained independently from the same set of refractive indices but at different forms.

III. EXPERIMENT

We measured the refractive indices of E7 in the visible spectral region using a multiwavelength Abbe refractometer and measured the refractive indices at $\lambda = 1.55$ and 10.6 μm using the wedged LC cell refractometer method, respectively.

A. Measurements at the visible-light spectrum

We measured the refractive indices of E7 using a multiwavelength Abbe refractometer (Atago DR-M4) at $\lambda = 450$, 486, 546, 589, 633, and 656 nm. The accuracy of the Abbe refractometer is up to the fourth decimal. For a given wavelength, we measured the refractive indices of E7 from 15 to 50 °C with a 5 °C interval. The temperature of the Abbe refractometer is controlled by a circulating constant-temperature bath (Atago Model 60-C3). The LC molecules are aligned perpendicular to the main and secondary prism surfaces of the Abbe refractometer by coating these two surfaces with a surfactant comprising of 0.294 wt % hexadecyletri-methyle-ammonium bromide (HMAB) in methanol solution. Both n_e and n_o are obtained through a polarizing eyepiece.

B. Measurements at $\lambda = 1.55$ and 10.6 μm

Figure 1 depicts the experimental apparatus for measuring the refractive indices of E7 at $\lambda = 1.55$ μm. A laser diode operating at the fundamental Gaussian mode was used as the light source. The laser was especially designed to be injected into an optical fiber. In order to obtain a free-propagating laser beam a collimator was connected to the output side of

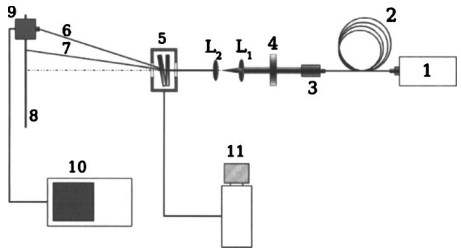

FIG. 1. The experimental apparatus for measuring the refractive indices at IR laser wavelengths. (1) Laser source. (2) Optical fiber. (3) Beam collimator. (4) Polarizer. (5) Thermostat containing the wedged LC cell. (6) Extraordinary beam. (7) Ordinary beam. (8) Micrometric track. (9) Pointlike detector. (10) Digital oscilloscope. (11) Temperature controller. L_1 and L_2 are two confocal lenses acting as a beam condenser.

the optical fiber. The laser beam was linearly polarized by means of a polarizer and the polarization axis was 45° with respect to the LC directors. The beam diameter was condensed to ~1 mm by two confocal lenses (L_1 and L_2) shown in Fig. 1. To form a wedged LC cell, two ITO (indium-tin-oxide) glass substrates were separated by two spacers having different thicknesses. The wedge angle was measured by an optical method to be $\theta = 0.040\,17$ rad with a precision of 6×10^{-5} rad.

The alignment of the LC inside the cell is planar which was obtained by buffing the spin-coated polyvinyl alcohol layer. Good LC alignment was obtained by inspecting the cell under a polarizing optical microscope. During experiments, the front substrate was arranged to be normal to the incoming infrared laser beam. The wedged cell was enclosed inside a thermostat and the sample temperature was controlled within 0.1 °C accuracy. A pointlike detector designed for operation at $\lambda = 1.55$ μm was mounted on a micrometric track. Under such condition, the detector can be moved up and down with a very precise control of its position. The position of the refracted laser beam is easily detected by moving the detector on the track. The detector signal is displayed on a LeCroy digital oscilloscope. The measurement principle consists of the evaluation of the deviation angle experienced by the laser beam due to the refraction of the beams by the LC material. In fact, when the laser beam passes through the wedged LC cell it undergoes a splitting process, and two beams (ordinary and extraordinary) emerge from the cell. The refractive indices are then retrieved by using the Snell law and simple geometrical calculations. The little shifts due to the presence of the glass substrates are also taken into account. The accuracy on the measurement of the refractive indices is estimated to be ~0.7%.

The experimental apparatus used for the measurement at 10.6-μm wavelength is analogous to the aforementioned one. The laser source is a continuous-wave (CW) CO_2 laser that operates on the fundamental Gaussian mode at $\lambda = 10.6$ μm (line P20). The detector used is the infrared pyroelectric video camera (Spiricon Pyrocam III, model PY-III-C-A). The two glass substrates of the wedged cell are now replaced by two ZnSe plates that allow the transmission of the CO_2 laser beam. More details about the experimental method and the experimental apparatus at 10.6-μm wavelength can be found in Ref. 18. In this case the estimated accuracy on the refractive indices is 0.5%.

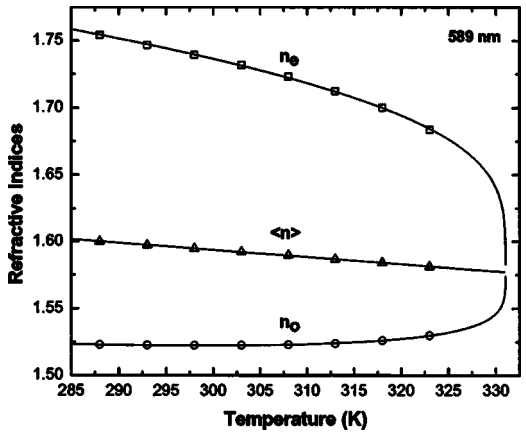

FIG. 2. Temperature-dependent refractive indices of E7 at $\lambda = 589$ nm. The open squares and circles represent the n_e and n_o measured at $\lambda = 589$ nm using the multiwavelength Abbe refractometer, respectively. The open upward triangles are the average refractive index $\langle n \rangle$ calculated by the experimental data. The solid curves are the fittings using the four-parameter model [Eqs. (6a) and (6b)]. The fitting parameters $[A, B, (\Delta n)_o, \beta]$ are $[1.7546, 5.36 \times 10^{-4}, 0.3768, 0.2391]$. The solid straight line is the fitting using Eq. (5). The fitting parameters $[A, B]$ are $[1.7456, 5.36 \times 10^{-4}]$.

IV. RESULTS AND DISCUSSIONS

The refractive indices of E7 were measured at $\lambda = 450$, 486, 546, 589, 633, and 656 nm in the temperature range from 15 to 50 °C with a 5 °C interval and at $\lambda = 1.55$ and 10.6 μm, respectively. Figure 2 depicts the temperature-dependent refractive indices of E7 at $\lambda = 589$ nm. The open squares, circles, upward triangles represent n_e, n_o, and average refractive index $\langle n \rangle$ for E7, respectively. The solid curves are the fitting results using Eqs. (6a) and (6b). The fitting parameters $[A, B, (\Delta n)_o, \beta]$ are $[1.7546, 5.36 \times 10^{-4}, 0.3768, 0.2391]$. The solid straight lines are the fitting results using Eq. (5). The fitting parameters $[A, B]$ are $[1.7546, 5.36 \times 10^{-4}]$. Clearly, the average refractive index decreases linearly as the temperature increases.

Next, we use the extended Cauchy model to fit the refractive indices n_e and n_o measured at the above-mentioned visible wavelengths and temperature range. Then we get the six Cauchy coefficients $[A_e, B_e, C_e]$ and $[A_o, B_o, C_o]$ for n_e and n_o, respectively. In Table I, we show the fitting parameters $[A_e, B_e, C_e]$ and $[A_o, B_o, C_o]$ for the extended Cauchy model [Eqs. (2a) and (2b)] in the temperature range from 15 to 50 °C by using the experimental data measured in the visible spectrum.

Figure 3 depicts the wavelength-dependent refractive indices of E7 at $T = 25$ °C. The open squares and circles represent the n_e and n_o of E7 in the visible region while the downward and upward triangles stand for the measured data at $\lambda = 1.55$ and 10.6 μm, respectively. The solid curves are the fittings to the experimental n_e and n_o data in the visible spectrum by using the extended Cauchy model [Eqs. (2a) and (2b)]. The fitting parameters are listed in Table I. In Fig. 3, we extrapolate the extended Cauchy model to the near- and far-infrared spectra. The extrapolated lines almost strike through the center of the experimental data measured at $\lambda = 1.55$ and 10.6 μm. The largest difference between the extrapolated and experimental data is only 0.4%. Considering the experimental error in the wedged cell refractometer

TABLE I. Fitting parameters for the extended Cauchy model [(Eqs. (2a) and (2b)] at different temperatures (in °C) by using the experimental data measured at visible wavelengths (in μm).

Temperature (°C)	n_e			n_o		
	A_e	B_e (μm^2)	C_e (μm^4)	A_o	B_o (μm^2)	C_o (μm^4)
15	1.7055	0.0087	0.0028	1.5006	0.0065	0.0004
20	1.6993	0.0085	0.0027	1.4998	0.0067	0.0004
25	1.6933	0.0078	0.0028	1.4994	0.0070	0.0004
30	1.6846	0.0090	0.0025	1.4989	0.0072	0.0004
35	1.6761	0.0091	0.0025	1.4987	0.0071	0.0004
40	1.6662	0.0091	0.0024	1.5033	0.0049	0.0008
45	1.6565	0.0083	0.0024	1.5018	0.0068	0.0006
50	1.6395	0.0095	0.0020	1.5062	0.0063	0.0006

method, the agreement between experiment and theory is very good. Figure 3 also indicates that the refractive indices will saturate in the far infrared region. The extended Cauchy model predicts that n_e and n_o would saturate to A_e and A_o in the long IR wavelength, respectively. For E7, the measured (n_e, n_o) at $\lambda = 10.6$ μm are (1.6914,1.4936) while the fitting parameters (A_e, A_o) are (1.6933,1.4994). The difference is less than 0.38%.

Temperature-dependent refractive indices are important for practical applications, such as projection displays and thermal-induced photonic band-gap tuning. It is highly desirable to predict the refractive indices at the designated operating temperature of a LC device, especially in the IR region. Here, we extrapolate the IR refractive indices using the extended Cauchy model and compare with those measured directly at $\lambda = 1.55$ and 10.6 μm at $T = 15$, 20, 25, 30, 35, 40, 45, and 50 °C, respectively. Then by using the four-parameter model [Eq. (6)] to fit the extrapolated data at $\lambda = 1.55$ and 10.6 μm, we obtain the refractive indices n_e and n_o in the whole nematic phase range at these two wavelengths.

Figure 4 depicts the temperature-dependent refractive indices of E7 at $\lambda = 1.55$ μm. The open circles are the n_e and n_o extrapolated from the extended Cauchy model. The open triangles are the average refractive index $\langle n \rangle$ calculated from the extrapolated n_e and n_o. The solid curves are the fittings using the four-parameter model [Eqs. (6a) and (6b)]. The solid straight line is the fitting using Eq. (5). The fitting parameters are listed in Table II. The filled circles are the refractive indices measured by the wedged LC cell refractometric method. The filled triangles are the average refractive index $\langle n \rangle$ calculated from the experimental data. In Fig. 4, excellent agreement among the extended Cauchy model, four-parameter model, and measured experimental data is found. The difference between the predicted values and the experimental data is less than 0.38%. The difference may be caused partly by the measurement error and by the local molecular overtone vibration bands. In Fig. 4, the average refractive index $\langle n \rangle$ decreases linearly as the temperature increases. In the isotropic phase range, n_e equals to n_o and the anisotropy vanishes. The refractive index in the isotropic phase also decreases linearly as the temperature increases.

Figure 5 depicts the temperature-dependent refractive indices of E7 at $\lambda = 10.6$ μm. The open circles represent the extrapolated n_e and n_o from the experimental data measured at visible wavelengths using the extended Cauchy model.

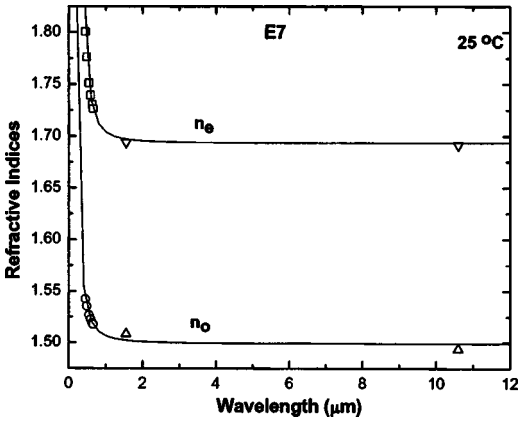

FIG. 3. Wavelength-dependent refractive indices of E7 at $T = 25$ °C. The open squares and circles are the n_e and n_o of E7 measured at the visible spectrum. The solid curves are the fittings to the experimental data measured at the visible spectrum by using the extended Cauchy model [Eqs. (2a) and (2b)]. The fitting parameters are listed in Table I. The downward and upward triangles are n_e and n_o of E7 measured at $T = 25$ °C and $\lambda = 1.55$ and 10.6 μm, respectively.

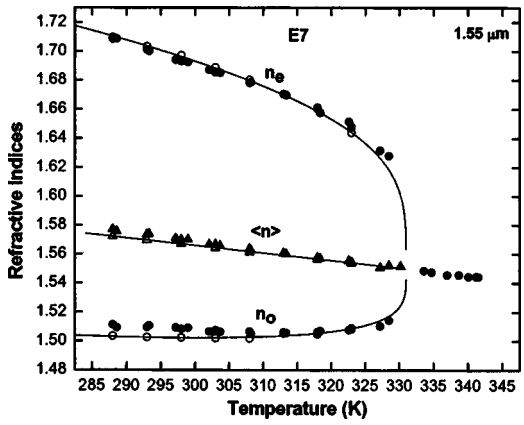

FIG. 4. Temperature-dependent refractive indices of E7 at $\lambda = 1.55$ μm. The filled circles are the refractive indices n_e and n_o measured by the wedged LC cell method. The filled triangles are the average refractive index $\langle n \rangle$ calculated by the experimental data. The open circles are the n_e and n_o extrapolated from the experimental data measured at visible spectrum using the extended Cauchy model. The open triangles are the average refractive index $\langle n \rangle$ calculated by the extrapolated n_e and n_o. The solid curves are fittings using Eqs. (6a) and (6b). The solid straight line is the fitting using Eq. (5). The fitting parameters are listed in Table II.

TABLE II. Fitting parameters for the average refractive index $\langle n \rangle$ and birefringence (Δn) of E7 at $\lambda = 1.55$ and 10.6 μm calculated by the extrapolated refractive indices from the visible spectrum.

	$\langle n \rangle$		Δn	
λ (μm)	A	B (K^{-1})	$(\Delta n)_o$	β
1.55	1.7230	5.24×10^{-4}	0.3485	0.2542
10.6	1.7201	5.25×10^{-4}	0.3499	0.2579

The open triangles are the average refractive index $\langle n \rangle$ calculated by the extrapolated n_e and n_o. The solid curves are the fittings using the four-parameter model [Eqs. (6a) and (6b)]. The solid straight line is the fitting using Eq. (5). The fitting parameters are listed in Table II. The filled circles are the refractive indices n_e and n_o measured by the wedged cell refractometer method. The filled triangles are the average refractive index $\langle n \rangle$ calculated by the experimental data. In Fig. 5, excellent agreement among the extended Cauchy model, four-parameter model, and experimental data is found. The difference between the theoretical values and the experimental data is less than 0.4%. The difference may result from the local molecular vibrations. In the low IR region, several molecular vibration bands exist. Because of relatively weak oscillator strength, their contribution to the refractive indices is localized. In Fig. 5, the average refractive index $\langle n \rangle$ decreases linearly as the temperature increases.

Overall, the difference between the predicted model values and experimental data measured by the wedged cell refractometer method is less than 0.4%. Taking into account the measurement errors and the effects of local molecular vibration bands, such a small difference is acceptable. That means, the extrapolated IR refractive indices from those measured by the Abbe refractometer (visible wavelengths) and those measured directly from the wedged cell refractometer at discrete IR laser wavelengths are consistent. The advantages of using Abbe refractometer are twofold: it is easy to use and less time consuming.

V. CONCLUSIONS

We have measured the refractive indices of E7 in the visible, near, and far IR spectral regions. In the visible region, a multiwavelength Abbe refractometer was proven to be powerful and accurate. In the near IR ($\lambda = 1.55$ μm) and long IR ($\lambda = 10.6$ μm) regions, the LC refractive indices can be measured using a wedged cell refractometer method. These data can be fitted smoothly by the extended Cauchy model.

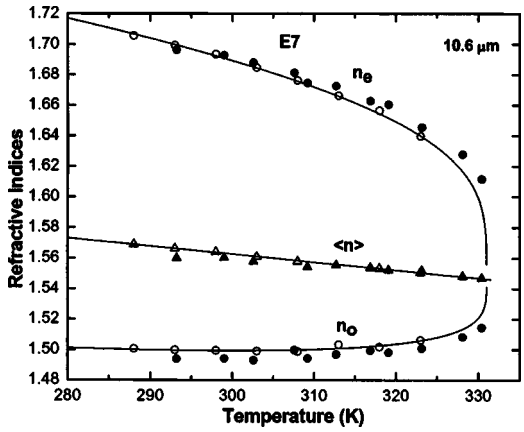

FIG. 5. Temperature-dependent refractive indices of E7 at $\lambda = 10.6$ μm. The filled circles are the refractive indices n_e and n_o measured by the wedged LC cell refractometer method. The filled triangles are the average refractive index $\langle n \rangle$ calculated by the experimental data. The open circles represent the n_e and n_o extrapolated from the experimental data measured at visible spectrum using the extended Cauchy model. The open triangles are the average refractive index $\langle n \rangle$ calculated by the extrapolated n_e and n_o. The solid curves are the fittings using Eqs. (6a) and (6b). The solid straight line is the fitting using Eq. (5). The fitting parameters are listed in Table II.

ACKNOWLEDGMENTS

The UCF group is indebted to the financial support of AFOSR under Contract No. F49620-01-1-0377, and the Italy group would like to thank Dolcetti Antonietta for her kind help.

[1] S. T. Wu, U. Efron, and L. D. Hess, Appl. Phys. Lett. **44**, 1033 (1984).
[2] S. Brugioni and R. Meucci, Opt. Commun. **230**, 19 (2004).
[3] U. Efron, S. T. Wu, J. Grinberg, and L. D. Hess, Opt. Eng. **24**, 111 (1985).
[4] R. M. Matic, Proc. SPIE **2120**, 194 (1994).
[5] P. F. McManamon *et al.*, Proc. IEEE **84**, 268 (1996).
[6] T. T. Alkeskjold, A. Bjarklev, D. S. Hermann, and J. Broeng, Opt. Express **11**, 2589 (2003).
[7] T. T. Alkeskjold, J. Laegsgaard, A. Bjarklev, D. S. Hermann, J. Broeng, J. Li, and S. T. Wu, Opt. Express **12**, 5857 (2004).
[8] D. Dolfi, M. Labeyrie, P. Joffre, and J. P. Huignard, Electron. Lett. **29**, 926 (1993).
[9] K. C. Lim, J. D. Margerum, and A. M. Lackner, Appl. Phys. Lett. **62**, 1065 (1993).
[10] S. T. Wu, U. Efron, and L. D. Hess, Appl. Opt. **23**, 3911 (1984).
[11] M. Warenghem and G. Joly, Mol. Cryst. Liq. Cryst. **207**, 205 (1991).
[12] R. J. Mansfield, MS thesis, Pennsylvania State University, 1990.
[13] S. Brugioni, S. Faetti, and R. Meucci, Liq. Cryst. **30**, 927 (2003).
[14] S. T. Wu, J. Appl. Phys. **84**, 4462 (1998).
[15] S. T. Wu, Phys. Rev. A **33**, 1270 (1986).
[16] S. T. Wu, C. S. Wu, M. Warenghem, and M. Ismaili, Opt. Eng. **32**, 1775 (1993).
[17] J. Li and S. T. Wu, J. Appl. Phys. **95**, 896 (2004).
[18] J. Li and S. T. Wu, J. Appl. Phys. **96**, 170 (2004).
[19] J. Li, S. Gauza, and S. T. Wu, Opt. Express **12**, 2002 (2004).
[20] I. Haller, Prog. Solid State Chem. **10**, 103 (1975).
[21] J. Li, S. Gauza, and S. T. Wu, J. Appl. Phys. **96**, 19 (2004).